A Theoretical Study of the Dynamics of the S + *c*-C_3H Reaction

J. R. Flores,*,† E. Martínez-Núñez,‡ S. A. Vázquez,‡ and F. J. Gómez†

Departamento de Química Física, Facultade de Ciencias, Universidade de Vigo, Lagoas-Marcosende, 36200 Vigo, Spain and Departamento de Química Física, Facultade de Química, Universidade de Santiago de Compostela, 15706 Santiago de Compostela, Spain

Received: May 15, 2002; In Final Form: July 17, 2002

A theoretical study of the dynamics of the S + *c*-C_3H reaction was carried out, following a theoretical approach in which the reaction is decomposed in two steps: the collision process and the evolution of the reaction intermediate formed in the reactive collisions. In both steps, classical dynamical methods were employed. For the collision step, we used an analytical potential energy surface in conjunction with a Hamiltonian based on the adiabatic capture centrifugal sudden approximation, whereas for the second step, we computed direct trajectories with a hybrid analytical and MNDO-type potential energy surface with specific reaction parameters. We calculated capture rate coefficients for the temperature interval [60−600 K] as well as branching ratios for $T = 100$ and 300 K. Our results suggest that the overall reaction rate is quite high but also that production of SC_3 + H may have a branching ratio of about 50%, SC + C_2H being the other main product. The results were compared to those of a similar study of the S + *l*-C_3H reaction.

Introduction

Sulfur-containing cumulenes SC_n ($n = 1-3, 5$), which appear in the form of linear S−C_n chains, are of considerable astrophysical importance and have been received considerable theoretical and experimental attention.[1−7] Among the experimental work, we would cite the Fourier transform microwave studies by the groups of Lovas,[2] Oshima,[3] Hirahara,[4] Kasai,[5] and Saito[6] as well as the Fourier transform infrared absorption spectra recorded by Vala and co-workers[7] and also by Maier and co-workers in the case of SC_3.[8] The sulfur-bearing cumulenes have also been the subject of intense theoretical work. Lee[9] studied many linear SC_n systems through a (density functional) BLYP method, whereas Vala and co-workers[7] used both the B3LYP and MP2 (second-order Møller−Plesset) methods. Maclagan and Sudkeaw[10] computed the ionization potential and proton affinities of SC_2 and SC_3, whereas Peeso et al.[11] and two of us[12] studied the excited states of SC_3. Murakami[13] computed spectroscopic properties of the ground states of SC_n, $n = 1-3$. Botschwina, Maier, and co-workers made a detailed theoretical study of SC_3.[14]

It has been advocated that neutral−neutral reactions may play an important role in the production of sulfur bearing carbon chains.[15,16] It has been argued that SC_3 could be generated by the reaction between sulfur and C_3H:[15,16]

$$S + C_3H \rightarrow SC_3 + H$$

However, its rate coefficient and the fact that other products may be formed are unknown. The C_3H radical could be either in a linear form ($^2\Pi$) or in a state with a C_3 cycle ($^2B_2$), with the latter being the ground state. The ground state of SC_3 is linear ($^1\Sigma^+$). Two of us have studied the lowest doublet and quartet potential energy surface (PES) of the SC_3H system[17] as well as the energy profiles of a number of doublet and quartet states for the interaction of sulfur with both *l*-C_3H and *c*-C_3H. In addition, we have performed a theoretical study of the dynamics of the S + *l*-C_3H reaction.[18] That work employed classical trajectory methods in combination with an analytical PES for the study of the collisions, and with a (MNDO-type) PM3[19] surface with specific reaction parameters (PM3-SRP),[20−23] for the study of the evolution of the SC_3H complex formed in the collision. In the latter case, the trajectories were of the direct dynamics type. The most important conclusion of that study is that the branching ratio corresponding to the production of SC_3 might not be very high; we bracketed it between 52% and 24% ($T = 300$ K). Even though the capture rate is not very small $k_c(300\ \text{K}) = 2.1 \times 10^{-10}$ cm^3 s^{-1}, it is not guaranteed that the overall rate for the generation of SC_3 is high enough for this process to have a strong impact in the generation of SC_3. The obvious complement to our previous study is the analysis of the S + *c*-C_3H reaction (*c*-C_3H stands for $C_3H(^2B_2)$), which we present in this paper. It must be noted that *c*-C_3H is found to be much more abundant than the linear form in some sources, particularly in dark clouds;[24] the likely reason being the dynamical behavior of the C + C_2H_2 reaction.[25,26]

Computational Methods

Our dynamical study relies on a previous work by two of us on the lowest doublet and quartet PES of the SC_3H system.[17] That study was performed basically at the QCISD(T)/6-311+G(3df,2p)//QCISD/6-311G**+ZPE(B3LYP/6-311G**)[27−30] level, but some empirical corrections were included that made the relative energies of G2(QCI)[31] quality. Besides, we computed some energy profiles of a number of doublet and quartet states for the interaction of sulfur with both *l*-C_3H and *c*-C_3H; this information is important in order to correct the capture rates by the fraction of the PES that is attractive.[32]

In the present work, we split the reaction dynamics into two parts for which we apply different methods: the capture or collision step and the unimolecular step. These methods will

* To whom correspondence should be addressed. E-mail: flores@uvigo.es.
† Universidade de Vigo.
‡ Universidade de Santiago de Compostela.

10.1021/jp021215t CCC: $22.00
Published on Web 08/16/2002

CHART 1: Schematic Representation of the Potential Surface of the S + C_3H reaction. The relative energies (in kcal mol^{-1}) have been computed at the QCISD(T)/6-311+G(3df,2p)//QCISD/6-311G + ZPVE(B3LYP/6-311G**) with the corrections described in ref 17: S + *l*-C_3H (0), S + *c*-C_3H (−4.5), M1 (−120.5), M2 (−103.4), M3 (−75.0), M4 (−73.0), TS12 (−37.8), TS23 (−45.3), TS34 (−43.6), TS1H (−51.8), TS3H (−43.5), TS4H (−48.9), SC_3 + H (−52.9), SC + C_2H (−40.0). Reactants and Products Are in Their Electronic Ground States.**

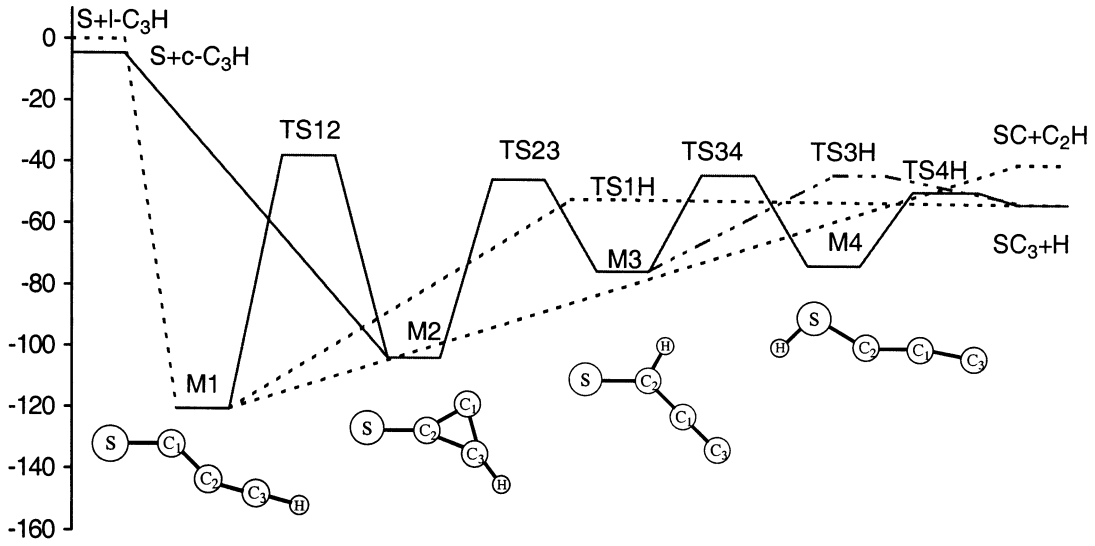

be described after we present the most salient features of the PES of the SC_3H system.

A. PES of the SC_3H System. The PES of the SC_3H system was already described in ref 17. Here, we will only pay attention to the most relevant features with the help of Chart 1 and Figure 1. The reaction of S with *l*-C_3H or *c*-C_3H is exothermic for the generation of $SC(^1\Sigma^+)$ + $C_2H(^2\Sigma^+)$ and $SC_3(^1\Sigma^+)$ + $H(^2S)$. The results of a study of the excited states of SC_3[12] indicate that none of them can be easily formed in these reactions, for the reaction would be endothermic, although at least the lowest-lying excited state of C_2H (^2A in linear geometries) could be formed.[33] The collisions of S and *c*-C_3H will initially give an energized M2 species

$$S + c\text{-}C_3H \rightarrow M2$$

M2 may dissociate back into the reactants

$$M2 \rightarrow S + c\text{-}C_3H \qquad (1)$$

or transform into M3 or M4, which may both generate $SC_3(^1\Sigma^+)$ through bond fission processes exhibiting transition states:

$$M2 - TS23 \rightarrow M3 - TS3H \rightarrow SC_3(^1\Sigma^+) + H \qquad (2)$$

$$M2 - TS23 \rightarrow M3 - TS3H \rightarrow M4 - TS4H \rightarrow SC_3(^1\Sigma^+) + H \qquad (3)$$

M2 may also isomerize into M1, which is a nearly-linear SCCCH adduct[34] that may generate $SC_3(^1\Sigma^+)$ and also $SC(^1\Sigma^+)$ + $C_2H(^2\Sigma^+)$:

$$M2 - TS12 \rightarrow M1 - TS1H \rightarrow SC_3(^1\Sigma^+) + H \qquad (4)$$

$$M2 - TS12 \rightarrow M1 \rightarrow SC(^1\Sigma^+) + C_2H(^2\Sigma^+) \qquad (5)$$

M1 might also fragment into S + *l*-C_3H even though *l*-C_3H is higher in energy than *c*-C_3H:

$$M1 \rightarrow S + l\text{-}C_3H \qquad (6)$$

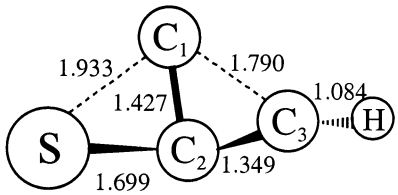

<HC$_3$C$_2$ = 130.2 °; <HC$_3$C$_2$C$_1$ =-81.0 °

<SC$_2$C$_1$C$_3$ = 142.2 °

TS12

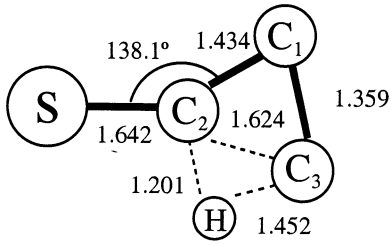

TS23

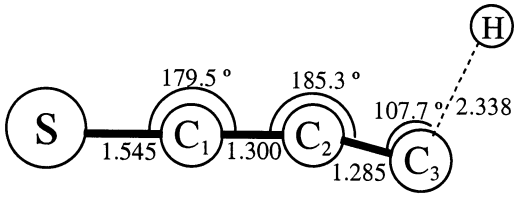

TS1H

Figure 1. QCISD/6-311G** geometries (Å and degrees) of the most relevant saddle points.

Obviously, M2 may be formed again from M1 via TS12, not just directly from the reactants, giving much more complex mechanisms; however, they are less frequent than the direct mechanisms. The crucial transition states are only those depicted in Figure 1, namely, TS12, TS23, and TS1H (see ref 17 for

details). The reason is that we will approximate the unimolecular dynamics by assuming that if TS23 is reached the trajectory will finally produce SC_3 + H. It is interesting to note that the reaction coordinate corresponding to TS12 implies that some sort of C-atom scrambling takes place during the M1 ↔ M2 isomerization, as shown in Chart 1; the carbon atom bonded to sulfur in M2 becomes the central carbon in M1. Note also that the C_2-C_1 and C_2-C_3 bonds are preserved in this rearrangement. Finally, TS23 involves hydrogen migration from C_3 to C_2 and simultaneous breaking of the C_2-C_3 linkage, C_2 keeps its bond with sulfur.

B. Capture Step. The capture step is treated through the classical trajectory method, where the coordinates are the distance between sulfur and the center of mass of the c-C_3H group and the three rotation angles of the latter. The corresponding Hamiltonian is written as follows:

$$H = \frac{p_r^2}{2\mu} + V_{\min}(r) + \frac{|\vec{J} - \vec{j}|^2}{2\mu r^2} + H_{\rm rot} + V_o(r,\theta,\psi) \quad (7)$$

The vectors $\vec{J}$ and $\vec{j}$ represent respectively the total angular momentum of the collision and the angular momentum of the rotation of the c-C_3H group. $V_{\min}(r)$ is the minimum of the potential for a particular value of r, the distance between the centers of mass. $V_o(r,\theta,\psi)$ represents the orientation potential; thus, the total potential would be $V_{\rm cap}(r,\theta,\psi) = V_{\min}(r) + V_o(r,\theta,\psi)$. θ represents the angle of the dipole moment with respect to the line connecting the centers of mass defined such that when it is zero sulfur is on the side of the hydrogen atom. ψ is the angle of rotation of c-C_3H about its symmetry axis. μ is the reduced mass of the collision, and p_r is the momentum associated with the coordinate r. $H_{\rm rot}$ is the Hamiltonian corresponding to the rotation of the c-C_3H group. We have employed two equivalent expressions in terms of the Euler 313 and 123 sets, as shown in the Appendix.

The value of the centrifugal term is determined by using to the centrifugal sudden approximation[35]

$$\frac{|\vec{J} - \vec{j}|^2}{2\mu r^2} = \hbar^2[J(J+1) - 2M + j(j+1)]/2\mu r^2 \quad (8)$$

We split the potential into short and long-range parts

$$V_{\rm cap} = (V_{\rm m} + V_{\rm d})w + V_{\rm lr}(1 - w) \quad (9)$$

where $V_{\rm lr}$ is the long-range potential, $V_{\rm m} + V_{\rm d}$ is the short-range potential, and w is a switching function, which is defined as follows:

$$w = 1/\{1 + \exp[-\gamma/(r_{\rm SC} - r_{\rm SC}^{\rm eq})^2]\exp[b(r_{\rm SC} - r_{\rm SX})]\} \quad (10)$$

where $r_{\rm SC}$ is the smallest distance between sulfur and any of the carbon atoms not bonded to hydrogen in c-C_3H, $r_{\rm SC}^{\rm eq}$ is the corresponding equilibrium distance, and $r_{\rm SX}$ is a parameter. $V_{\rm m}$ is basically a Morse-type potential defined in the following way:

$$V_{\rm m} = V_1 + V_2 + V_{\rm H} \quad (11)$$

where V_1 reads

$$V_1 = -\{D_e - D_e[1 - \exp(-\beta(r_{\rm SC1} - r_{\rm SC}^{\rm eq}))]^2\} \exp[-f(\theta_p - \theta_0)^2] + F_1 \exp[-f_1(r_{\rm SC1} - r_{\rm SC}^{\rm eq})^4](\theta_p - \theta)^2 \exp[-f(\theta_p - \theta_0)^2] \quad (12)$$

V_2 has the same form but in terms of $r_{\rm SC2}$ and $\theta_p + \theta_0$ (where $\theta_p = \pi - \theta$) instead of $r_{\rm SC1}$ and $\theta_p - \theta_0$, respectively, and $V_{\rm H}$, which accounts for the sulfur−hydrogen repulsion, has the following expression

$$V_{\rm H} = A_{\rm H} \exp[-f_{\rm H}(|\theta_p| - \pi)^2] \exp(-\beta_{\rm H} r_{\rm SH}^2) \quad (13)$$

$r_{\rm SH}$ represents the sulfur−hydrogen distance. Note that $V_{\rm m}$ takes care of the fact that two S−C bonds can be formed when sulfur approaches c-C_3H and gives an adequate dependence on θ_p.

$V_{\rm d}$ in eq 9 accounts for the variation of the short-range potential with ψ, the angle of rotation of c-C_3H about its symmetry axis. It has the following form

$$V_{\rm d} = V_0|e^{-A_p(r_{\rm SC1} - r_{\rm SC,d})^2} e^{-A_t(\theta_p - \theta_0)^2} - e^{-A_p(r_{\rm SC2} - r_{\rm SC,d})^2} e^{-A_t(\theta_p + \theta_0)^2}| \sin^2\psi \quad (14)$$

where V_0, A_p, $r_{\rm SC,d}$, A_t, and θ_0 are parameters and ψ is defined such that it is valued $n\pi$ for planar arrangements ($n = 0, 1, ...$). Note that $V_{\rm d}$ is exactly zero when $\theta_p = 0$, and with the parameters employed, it is virtually zero for $\theta_p = \pi$.

We employ two versions of the short-range potential $V_{\rm m}$, named $V_{\rm m,I}$ and $V_{\rm m,II}$, which differ from each other only in the value given to the D_e parameter of V_1 and would give two representations of $V_{\rm cap}$, denoted as $V_{\rm cap.I}$ and $V_{\rm cap,II}$. In the first case, D_e is given a value such that the potential represents the QCISD(T)/6-311+G(3df,2p) dissociation energy,[17] whereas in the second case, it models the dissociation energy of a QCISD-(T)/6-311+G(3df,2p) energy profile computed with a geometry of c-$C_3H(^2B_2)$ which was optimized at the QCISD/6-311G** level and which was *not* allowed to relax. We assume that the difference between the energies of the minima of the two potentials may be a measure of the amount of vibrational energy the SC_3H complex acquires in its C_3H moiety as a result of the relaxation of the geometry of the C_3H group.

The long-range potential consists of induction, dispersion, and electrostatic terms, as defined by Buckingham:[36]

$$V_{\rm lr} = V_{\rm elec} + V_{\rm ind} + V_{\rm disp} \quad (15)$$

The electrostatic contribution includes dipole−quadrupole terms and is defined as follows:[37]

$$V_{\rm elec} = -\frac{1}{3}\sum_{i,j,k} T_{2,i,j,k}\mu_{1,i}\Theta_{2,j,k} \quad (16)$$

where the indices 1 and 2 refer to c-C_3H and S, respectively.

The components of the quadrupole moment are made dependent on $\{r,\theta\}$ through the following expression:

$$\Theta_{2,j,k} = \Theta^0_{2,j,k}[1 - w_Q(b_Q, r_{\rm SX}^Q)] \quad (17)$$

where w_Q is a switching function defined as in eq 10, but with different values for some of the parameters, namely, b_Q and $r_{\rm SX}^Q$. The role of this switching function is to activate the atomic quadrupole at short distances. The rationale of this approach, which has been discussed already in ref 38, is based on the fact that the three electron configurations corresponding to the ^3P term of sulfur should be essentially degenerate at long distances, providing an average null quadrupole. In other words, only at short distances there must be a clear preference for a particular orientation of the quadrupole, as we discuss below. It must be noted however that the quadrupole activation does not have a marked influence on the PES for $V_{\rm m} + V_{\rm d}$ of eq 9 dominates the short-range potential. For this reason, we

TABLE 1: Parameters of the PES Employed in the Capture Computations[a]

parameter	value	parameter	value
μ (c-C_3H)[b]	2.3359 D	f[f]	0.196 rad^{-2}
Q_{xx}(c-C_3H)[b]	−17.039 DÅ	F_1[f]	209000 J/mol
Q_{yy}(c-C_3H)[b]	−21.371 DÅ	f_1[f]	5.0 Å^{-4}
Q_{zz}(c-C_3H)[b]	−15.127 DÅ	θ_0[f]	0.9964 rad
α_{xx} (c-C_3H)[b]	22.411 au	A_H[e]	500000 J/mol
α_{yy}(c-C_3H)[b]	49.051 au	f_H[e]	0.80 rad^{-2}
α_{zz}(c-C_3H)[b]	32.509 au	β_H[e]	2.0 Å^{-2}
$Q_{xx}(S) = Q_{yy}(S)$[c,d]	−12.141 DÅ	V_0[e]	0.5 au
$Q_{zz}(S)$[c,d]	−15.218 DÅ	A_p[e]	0.290 Å^{-2}
$\alpha_{xx}(S) = \alpha_{yy}(S)$[c]	18.768 au	r_{SC}[e,f]	1.405 Å
$\alpha_{zz}(S)$[c]	22.811 au	A_t[e]	2.4 rad^{-2}
U_{12}[e]	105600 cm^{-1}	γ_w[e]	1 Å^2
$D_{e,I}$[f]	390370 J/mol	r_{SX}[e]	4.610 Å
$D_{e,II}$[f]	393947 J/mol	b[e]	10 Å^{-1}
β[f]	1.995 Å^{-1}	r_{SX}^{Q}[e]	6.0 Å
r_{SC}^{eq}[f]	1.609	b_Q[e]	4 Å^{-1}

[a] The values of the quadrupole moments correspond to the following definition $Q_{ij} = \sum_m e_m r_{i,m} r_{j,m}$. [b] B3LYP/aug-cc-pVTZ//B3LYP/aug-cc-pVTZ computation. [c] B3LYP/aug-cc-pVTZ. [d] "Fully activated" quadrupole components, i.e., they correspond to $\Theta_{2,j,k}^{(0)}$ of eq 10. [e] Obtained by fitting to the UCCSD(T)/6-311G** and RHF-UCCSD(T)/6-311G** energy profiles; the latter corrected for basis set superposition error. [f] Determined by means of QCISD(T)/6-311+G(3df,2p)//QCISD/6-311G** PES points.

considered the use of a switching function as a satisfactory procedure and discarded more elaborate approaches. Note also there is no need of such quadrupole activation in the case of c-C_3H.

The induction contribution includes dipole−induced dipole and quadrupole-induced dipole terms and can be written as follows:

$$V_{ind} = -\frac{1}{2}\sum_{i,j}\alpha_{2,i,j}\left(\sum_k T_{2,i,k}\mu_{1,k} - \frac{1}{3}\sum_{k,l} T_{2,i,k,l}\Theta_{1,k,l}\right)\left(\sum_k T_{2,j,k}\mu_{1,k} - \frac{1}{3}\sum_{k,l} T_{2,j,k,l}\Theta_{1,k,l}\right) - \frac{1}{2}\sum_{i,j}\alpha_{1,i,j}\left(\frac{1}{3}\sum_{k,l} T_{2,i,k,l}\Theta_{2,k,l}\right)\left(\frac{1}{3}\sum_{k,l} T_{2,j,k,l}\Theta_{2,k,l}\right) \quad (18)$$

The dispersion interaction includes induced dipole-induce dipole terms:

$$V_{disp} = -\frac{U_{12}}{4}\sum_{i,j,k,l} T_{2,i,j}T_{2,k,l}\alpha_{1,i,k}\alpha_{2,j,l} \quad (19)$$

where U_{12} is taken as an adjustable parameter. The indices $\{i,j,k,l\}$ stand for any of the Cartesian coordinates. The tensor operators are defined as follows:

$$T_{2,i,j} = (3r_i r_j - r^2\delta_{i,j})r^{-5}$$

$$T_{2,i,j,k} = -3[5r_i r_j r_k - r^2(r_i\delta_{j,k} + r_j\delta_{k,i} + r_k\delta_{i,j})]r^{-7} \quad (20)$$

where $\{r_i\}$ stand for the Cartesian components of the vector from the center of mass of 1 (c-C_3H) to 2 (the sulfur atom).

The parameters are given in Table 1. The treatment of the sulfur atom is a relatively important point. In principle, the free atom should be a spherical system in a ^3P electronic term; three axially symmetric and degenerate electron configurations would contribute equally to its wave function. The presence of c-C_3H introduces a perturbation that breaks the degeneracy. Choosing one particular electron configuration is equivalent to selecting one particular orientation of the atomic quadrupole, which also entails using a polarizability matrix coherent with this orientation. The important point we want to make is that the lowest-energy orientation of the atomic quadrupole varies depending on the orientation of the c-C_3H group. There are basically two options. The first would entail keeping one particular orientation of the sulfur quadrupole during the trajectory; this choice is consistent with following a diabatic PES. The second choice, which we would call adiabatic trajectory approach and is the one we followed in the final computations, is basically equivalent to keeping the trajectory on the lowest-lying surface; one does this at long range quite simply by picking the most favorable orientation of the atomic quadrupole at every point $\{r,\phi,\theta,\psi\}$. An alternative to this procedure would be an approach based on a very high-level multireference configuration interaction method for the computation of the PES at long distances, perhaps in combination with a direct dynamics approach to the trajectory computations. This kind of procedure would be not only terribly expensive in terms of computer resources but also not better, for other problems would arise related to the accuracy of the electronic energy computations at very long range and also with the parametrization of the PES (except if direct dynamics were performed).

The basic results of the capture step trajectory computations are the capture rate coefficients and approximate distributions of the total energy of the SC_3H complex. We have employed two models of these energy distributions.

Model A. In model A, we employ the following correlation:

$$\begin{bmatrix} \text{capture} & \text{complex} \\ \hbar^2[J(J+1) - 2M + j(j+1)]/2\mu r^2 & \rightarrow E_{rot,x,y} \\ E_{rot} - \frac{p_\psi^2}{2I_z} - \frac{p_\theta^2}{2}(\cos^2\psi/I_x + \sin^2\psi/I_y) & \rightarrow E_{rot,z} \\ \frac{p_\psi^2}{2I_z} + \frac{p_\theta^2}{2}(\cos^2\psi/I_x + \sin^2\psi/I_y) + V_o(r,\theta,\psi) & \rightarrow E_{b,S-C3H} \\ \frac{p_r^2}{2\mu r^2} & \rightarrow E_{s,S-C3H} \end{bmatrix}$$

The centrifugal energy correlates with the rotational energy of the complex, excluding the component that corresponds to the singular axis (z, roughly coincident with the S−C bond of the complex). The rotational energy of c-C_3H excluding the two components shown in the correlation scheme, which correspond to the θ and ψ angles of Euler's 313 set, correlates with the rotational energy about the z axis of the SC_3H complex. Finally, the terms in the third expression correlate with part of the vibrational energy of the SC_3H complex, particularly with that deposited in the S−C_3H bending normal modes, $E_{b,S-C3H}$, whereas $p_r^2/2\mu r^2$ correlates with the energy of the S−C stretching normal mode, $E_{s,S-C3H}$. The rest of the vibrational normal modes are given their zero-point energies, according to the vibrational frequencies of the potential employed in the unimolecular step. The trajectories are stopped when $r \leq 2.6$ Å, whereas $0 \leq \theta_p \leq \pi/2$. Then, the following adjustments are made: $V_o(r_s,\theta_s,\psi_s) - V_o(r_s,\theta_m',\psi_m')$ is added to $E_{b,S-C3H}$ term and $V_o(r_s,\theta_m',\psi_m') - V_o(r_m,\theta_m,\psi_m)$ is added to the $E_{s,S-C3H}$. $\{r_s,\theta_s,\psi_s\}$ are the coordinates of the point where the trajectory is stopped, $\{r_s,\theta_m',\psi_m'\}$ is the angular minimum corresponding to r_s (not a full minimum), and $\{r_m,\theta_m,\psi_m\}$ are the coordinates of the minimum. The trajectories were propagated by a fourth-order Runge−Kutta method with a time step of 0.5 fs.

Model B. It is quite similar to model A but some amount of energy is given to the normal modes of the C_3H group of the

SC_3H complex, in addition to their zero-point energy. In fact, the $V_{cap}(r_m,\theta_m,\psi_m)_I - V_{cap}(r_m,\theta_m,\psi_m)_{II}$ energy difference is added to the energy of the normal modes of the SC_3H complex with the exception of the S−C_3H stretching and bending modes. The rationale of this model is that this energy difference should be put into the vibrations of the C_3H group within the SC_3H complex, for it originates mostly in the distortion of the C_3H group during the formation of the S−C bond. Although we think that both models A and B tend to overestimate the percentage of energy deposited in the S−C_3H stretching and bending normal modes, where the latter should be, in principle, slightly less extreme. The criteria for halting trajectories and the rest of the technical details are the same as in model A.

Model C. In the third model proposed here, the same amount of vibrational energy as in model *A* is considered to be randomly distributed according to a microcanonical normal mode sampling (MNMS).[39] This procedure may underestimate the percentage of vibrational energy in the S−C_3H stretching; however, as shown below, the comparison between the results obtained with the other models and with this model may provide additional insights into the dynamical behavior of the SC_3H system. This model keeps the rotational energies $E_{rot,x,y}$ and $E_{rot,z}$ as obtained using model A. Note that, unlike models A and B, application of model C does not entail a capture computation as far as the vibrational energy is concerned.

C. Unimolecular Step. *1. The Semiempirical PM3-SRP Model*. The PES employed in the unimolecular part of the dynamics study V_{uni} is a combination of a PM3-SRP potential $V_{PM3-SRP}$ with some analytical functions

$$V_{uni} = V_{PM3-SRP}S_{C1C2}S_{C3H} + V_4(1 - S_{C3H}) + V_5(1 - S_{C1C2}) - D_{SC1}S_{SC1}S_{SC2} - D_{SC1c}S_{SC1}S_{SC2}S_{CCC} \quad (21)$$

where V_4 and V_5 comprise potential functions describing dissociation channels 4 and 5, respectively. Functions S_{C1C2}, S_{C3H}, S_{SC1}, and S_{SC2} depend on the C_1-C_2, C_3-H, $S-C_1$, and $S-C_2$ bond distances (for the atomic labeling see Chart 1), respectively, and S_{CCC} depends on the CCC bending angle, and are used to switch on the V_4 and V_5 long-range potentials and also to correct the S−C_3H dissociation energy.

A trial-and-error procedure was employed to fit the $V_{PM3-SRP}$ part of the potential to the ab initio energies[18] of M1, M2, TS12, and TS23. In addition, about 30 B3LYP/6-311G** points scaled with the QCISD(T)/6-311+G(3df,2p) dissociation energies were employed to guide the fitting of the intermolecular part of V4 and V5. In addition, the intramolecular potentials of the products were fitted to the available force fields. Finally, the more accurate ab initio dissociation energies[17] for channels 1 and 6 were employed in the determination of parameters D_{SC1} and D_{SC1c} in eq 21.

Although the explicit forms of the terms included in eq 21 were reported elsewhere,[18] here we briefly show them. Switching functions S_{C1C2} and S_{C3H} have the form

$$S_{C1C2} = \exp[-a(r_{C1C2} - r_{C1C2}^{eq})^b] \quad (22)$$

$$S_{C3H} = \exp[-a(r_{C3H} - r_{C3H}^{eq})^b] \quad (23)$$

with r_{C1C2}^{eq} and r_{C3H}^{eq} being the C_1-C_2 and C_3-H equilibrium distances of M1. Switching functions S_{SCX} (with X = 1,2) have the following form

$$S_{SCX} = 0.5\{1 + \tanh[e(r_{SCX} - r_{SC}^s)]\}\{1 - \exp[-f(r_{SCX} - r_{SC}^s)]\}^2 \quad (24)$$

with r_{SCX} being the SCX distance and r_{SC}^s a reference distance.

Asymptotic potentials (V_4 and V_5) have the following form:

$$V = D - \chi C_6/(r - r^{eq})^6 + V_{intra} \quad (25)$$

D is the reaction endothermicity for a given channel (4 or 5), χ are damping functions

$$\chi_4 = (1 - S_{C3H})^2 \quad (26)$$

$$\chi_5 = (1 - S_{C1C2})^2 \quad (27)$$

and r and r^{eq} in eq 25 are the C_3-H (C_1-C_2) bond distance and its equilibrium value at M1 in V_4 (V_5), respectively. Additionally, V_4 includes the term $g\exp[-h(r_{C3H} - r_{C3H}^{eq})]$ to reproduce saddle point TS1H. To guide the fitting of the parameters involved in V_4 and V_5, we used B3LYP/6-311G** points on the energy profiles of channels 4 and 5 and rescaled them with the more accurate QCISD(T) endothermicities.

The intramolecular potentials V_{intra} in eq 25 comprise the following harmonic functions fitted to the force field of the corresponding products

$$V_{SC} = 0.5k_{SC}(r_{SC} - r_{SC}^{eq,prod})^2 \quad (28)$$

$$V_{C_2H} = 0.5k_{CC}(r_{CC} - r_{CC}^{eq,prod})^2 + 0.5k_{CH}(r_{CH} - r_{CH}^{eq})^2 + 0.5k_{CCH}(\theta_{CCH} - \theta_{CCH}^{eq,prod}) \quad (29)$$

$$V_{SC3} = 0.5k_{SC1}(r_{SC1} - r_{SC}^{eq,prod})^2 + 0.5k_{C1C2}(r_{C1C2} - r_{C1C2}^{eq,prod})^2 + 0.5k_{C2C3}(r_{C2C3} - r_{C2C3}^{eq,prod})^2 + 0.5k_{SC1C2}(\theta_{SC1C2} - \theta_{SC1C2}^{eq,prod})^2 + 0.5k_{C1C2C3}(\theta_{C1C2C3} - \theta_{C1C2C3}^{eq,prod})^2 \quad (30)$$

where the bond distances, bond angles and their equilibrium values refer to the corresponding product molecules, except for the C−H distance, which, for simplicity, was given the same value as in M1.

The only modification made in the present work with respect to the model PES employed in our previous dynamics study[18] is the last term of eq 21, which corrects the S + c-C_3H dissociation energy. Particularly, function S_{CCC} reads

$$S_{CCC} = \{1 - \exp[-p(\theta - \theta_{eq})^2]\}^q \quad (31)$$

with θ being the CCC bending angle and $\theta_{eq} = \pi$ radians.

All of the parameters involved in the above unimolecular PES V_{uni} are gathered in Table 2. This PES predicts values in exact accord with the ab initio ones[17] for the S + c-C_3H, S + l-C_3H, SC + C_2H, and SC_3 + H dissociation asymptotes with respect to the minimum isomer M1. For dissociation channel 4, the saddle point of index one TS1H was also located in our model PES; its energy is 2 kcal mol^{-1} higher than that of the products (1.1 in the ab initio PES). The M1-M2 energy gap predicted by the model PES is 15.1 kcal mol^{-1}, which is in good agreement with the 15.9 kcal mol^{-1} predicted by QCISD(T) computations. These two isomers are connected by TS12, which lies 82 kcal mol^{-1} above M1 (vs 84 kcal mol^{-1} in the ab initio PES). In addition, in our model, potential TS23 lies 83 kcal mol^{-1} above M1 (77.3 kcal mol^{-1} from ab initio calculations). As mentioned above, in the dynamics part of this study, trajectories surmounting TS23 were considered to result in SC_3 + H; that is, recrossings through the TS23 dividing surface were not taken into account. The reason for this approximation stems from the fact that the first term in eq 21, which includes the semiempirical

TABLE 2: Parameters of the Full-Dimensional PES V_{uni}[a]

parameter	value	parameter	value
U_{ss} (H)	−13.000000	G_{pp} (C)	10.506292
β_s (H)	−5.500000	G_{p2} (C)	8.942566
Z_s (H)	1.067807	H_{sp} (C)	2.190980
α (H)	3.000000	U_{ss} (S)	−55.995371
G_{ss} (H)	14.894208	U_{pp} (S)	−43.592583
U_{ss} (C)	−49.800320	β_s (S)	−8.027465
U_{pp} (C)	−36.300000	β_p (S)	−7.291415
β_s (C)	−11.900015	G_{ss} (S)	9.164667
β_p (C)	−9.902755	G_{sp} (S)	6.585936
Z_s (C)	1.600000	G_{pp} (S)	9.868164
G_{ss} (C)	10.860708	H_{sp} (S)	3.941836
G_{sp} (C)	10.035027		
a	10 Å^{-6}	$r_{C2C3}^{eq,prod}$	1.287 Å
b	6	$\theta_{CCH}^{eq,prod}$	π rad
c	30 Å^{-6}	$\theta_{SC1C2}^{eq,prod}$	π rad
d	6	$\theta_{C1C2C3}^{eq,prod}$	π rad
e	12 Å^{-1}	k_{SC}	8.8 mdyn Å^{-1}
f	5 Å^{-1}	k_{CC}	16.4 mdyn Å^{-1}
g	50 kcal mol^{-1}	k_{CH}	6.43 mdyn Å^{-1}
h	2.5 Å^{-1}	k_{CCH}	0.05 mdyn
p	5	k_{SC1}	7.5 mdyn Å^{-1}
q	4	k_{C1C2}	2.0 mdyn Å^{-1}
r_{C1C2}^{eq}	1.413 Å	k_{C2C3}	15.76 mdyn Å^{-1}
r_{CH}^{eq}	1.060 Å	k_{SC1C2}	0.20 mdyn
r_{SC}^{s}	2.700 Å	k_{C1C2C3}	0.27 mdyn
$r_{SC}^{eq,prod}$	1.546 Å	D_{SC1}	27 kcal mol^{-1}
$r_{CC}^{eq,prod}$	1.216 Å	D_{SC1c}	18.3 kcal mol^{-1}
$r_{C1C2}^{eq,prod}$	1.298 Å		

[a] For the $V_{PM3-SRP}$ part of the potential, only those parameters that differ from its PM3 original value have been collected in this table.

TABLE 3: Initial Energy Partitioning for the Different Excitation Models Employed in the Unimolecular Decomposition of M2[a]

	$T = 300$ K			$T = 100$ K	
	model A	model B	model C[b]	model A	model C[b]
$E_{rot,x,y}$	2.7	2.6	2.7	1.2	1.2
$E_{rot,z}$	2.0	2.7	2.0	1.9	1.9
$E_{b,S-C3H}$	25.3	21.0	24.6	21.8	24.3
$E_{s,S-C3H}$	71.2	71.0	11.5	75.1	12.7
$E_{0,M2}$	12.5	18.5	72.9	12.5	72.4

[a] $E_{0,M2}$ represents the energy assigned to the normal modes other than the S−C_3H stretching ($E_{s,S-C3H}$) or bending ($E_{b,S-C3H}$) vibrations. Energies in kcal mol^{-1}. [b] Average values are listed.

part of the potential, becomes increasingly negligible as the C_3H distance increases, and therefore, additional analytical functions would be necessary to describe this part of the PES. This will result in a much more involved PES; however, for the purposes of the present study, the approximation followed here seems reasonable. The geometrical parameters and vibrational frequencies of the stationary points involved in the dynamics are reasonably well reproduced by the model PES and are not shown for simplicity.

2. Trajectory Computational Details. As indicated above, models A−C were employed to excite the M2 isomer of the SC_3H system by using the results of the capture step for two temperatures 100 and 300 K. Table 3 shows the energies deposited in the SCC bending modes (the two lowest ones) $E_{b,S-C3H}$, the S−C stretching mode $E_{s,S-C3H}$, the remaining modes $E_{0,M2}$ and in the rotation around the singular axis $E_{rot,z}$ and around the other two axes $E_{rot,x,y}$, at the two temperatures. For model C, average initial values for the above different energies are also listed in the table.

In this work, the trajectories were integrated in Cartesian coordinates, and no attempt was made to follow the ZPVE of the vibrational modes to investigate the possibility of ZPVE leakage. Channels 1 and 6 may experience some ZPVE leakage because their dissociation asymptotes are very near the excitation energy. Nevertheless, because the percentages of these processes are very small, as shown later, the overall conclusions will not change.

TABLE 4: Capture Rate Coefficients in Units of 10^{-10} cm^3 s^{-1} Scaled with the Fraction of PES Which Are Attractive (1/2)

	$k_c/10^{-10}$ cm^3 s^{-1}			$k_c/10^{-10}$ cm^3 s^{-1}	
T/K	model A	model B	T/K	model A	model B
600	4.5	4.2	180	3.4	3.2
300	3.7	3.5	140	3.3	3.1
260	3.6	3.4	100	3.0	2.9
220	3.4	3.2	60	2.8	2.7

For each set of initial conditions, 1000 trajectories were propagated by using the fourth-order Runge−Kutta−Gill algorithm, as implemented in a code that interfaces the classical trajectory program GENDYN[40] and the molecular orbital package MOPAC7.0[41] with a step size of 0.1 fs. The first derivatives of the PM3-SRP part of the PES were evaluated analytically using the Dewar−Liotard algorithm in MOPAC7.0. Analytical derivatives were also employed for the remaining part of the PES. The integration of the equations of motion was halted when the center-of-mass distance between the products of dissociation channels 1, 4, 5, or 6 reached 5 Å or when the trajectory surmounted TS23.

Results and Discussion

A. Capture Rates and Energy Distributions. The capture rate coefficients are presented in Table 4. The numbers were scaled by the fraction of PES that can be considered attractive according to the behavior of their energy profiles, reported in ref 17. The scaling fraction is $^1/_2$ (we have included the C^2A'' PES in the attractive set because of its crossing with the B^2A' PES, which generates a conical intersection). The capture rates computed with models A and B are very similar. The fact that model B employs a slightly more repulsive PES accounts for the smaller capture rates and the slightly higher average energies of the reactive collisions (see Table 3). There is very little dependence with temperature; the values increase a little with increasing temperature. These capture rates are higher than the ones computed for the S + *l*-C_3H reaction, which are bracketed between 2.1×10^{-10} cm^3 s^{-1} ($T = 300$ K) and 2.4×10^{-10} cm^3 s^{-1} ($T = 60$ K) and show a slight increase with decreasing temperature.[18] Even though providing reliable capture rates for lower temperatures, down to perhaps 10 K, would be convenient in order to assess more accurately the role of the present reaction in dark clouds, our method might not be accurate enough for such low temperatures. We do not expect a dramatic variation of the trend down to 10 K.

The evolution of the energy distributions of models A and B with temperature is displayed in Figures 2 and 3; the results for $T = 100$ and 300 K together with the MNMS results (model C) are shown in Table 3. It is readily seen that both models A and B agree in an accumulation of the energy in the S−C_3H stretching vibration of M2, although there is a moderate decrease with increasing temperature. The amount of energy deposited in the S−C_3H bending vibrations is normally higher than the energy of the other modes altogether and gets close to 20% at the higher temperatures. The rotational energy of M2 is only a small percentage of the total energy for low temperatures, but it increases strongly with temperature by virtue of the nearly

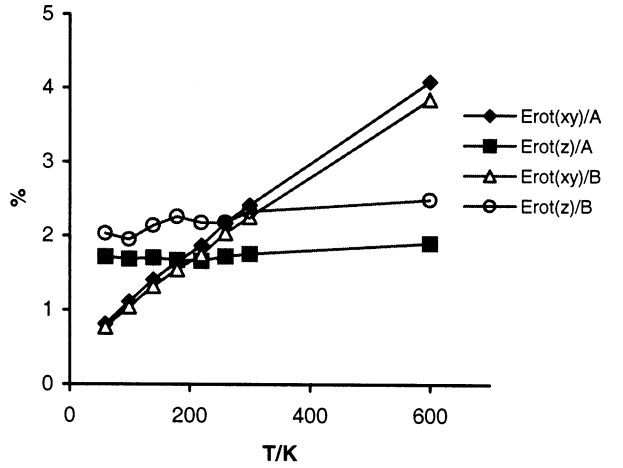

Figure 2. Rotational energy distribution as a function of the temperature for the capture models A and B.

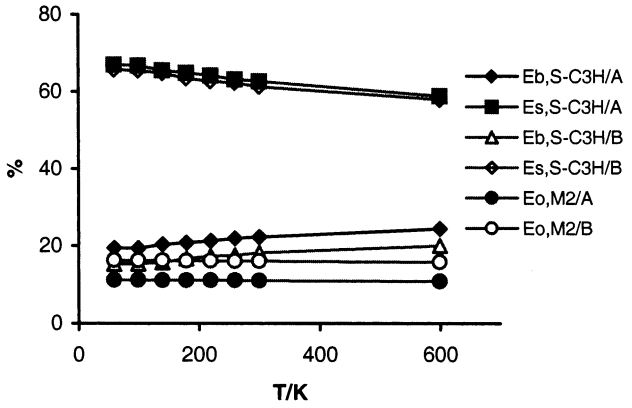

Figure 3. Vibrational energy distribution as a function of the temperature for the capture models A and B.

linear dependence of $E_{rot,xy}$ with the temperature. However, $E_{rot,z}$ is nearly constant and significantly lower for model B than for model A, probably as a result of a somewhat earlier locking of c-C_3H during the capture process in the case of model B. Inspection of Table 3 indicates that model C (MNMS) gives a completely different distribution of the vibrational energy (the rotational energies are the same as in model A), for the major part is deposited in the normal modes of M2 associated with the ring and C−H vibrations. The S−C_3H stretch has a very little energy, and its value is even lower than the one corresponding to the S−C_3H bending vibrations, which is very similar to that corresponding to model A. One could regard the energy distribution of model C as an *A*-type distribution in which the most of the energy of the S−C_3H stretch has been transferred to the normal modes of the C_3H moiety.

B. Analysis of the Unimolecular Step. Table 5 lists the branching ratios for the above-mentioned processes. In general, the branching ratios obtained under the three models are not very different from each other and suggest that production of SC_3 + H and SC + C_2H are competitive channels. With models A and C, SC_3 + H is the major product; 52% (A) and 54% (C) of the total reactions yield these products, whereas with model B, the SC + C_2H channel has the highest weight (52%). The three models predict the generation of S + l-C_3H or S + c-C_3H to be of little importance, especially the latter, which has, at the most, a weight of 1%. The results for 100 K are in very close agreement with those predicted for 300 K, pointing to a very weak temperature dependence of the branching ratios. We

TABLE 5: Branching Ratios in Percentages for the Processes Defined in the Text

	T = 300 K			T = 100 K	
process	model A	model B	model C	model A	model C
M2[a]/1	0	1	1	1	1
M3,M4[a]/2+3	45	38	43	46	44
M1[a]/4	7	6	11	6	10
M1[a]/5	45	52	42	43	42
M1[a]/6	3	3	3	4	3
2+3+4	52	44	54	52	54
4+5+6	55	61	56	53	55
[4/(4+5+6)][b]	13	10	20	11	18
[5/(4+5+6)][b]	82	85	75	81	76

[a] Intermediate whose fragmentation originates the products. [b] The percentages corresponding to the fragmentation of M1 in the S + l-C_3H reaction at T = 300 K are as follows:[18] 40% (SC_3 + H), 35%(SC + C_2H), 12%(S + l-C_3H) (*C*-type model, i.e., MNMS) and 5% (SC_3 + H), 71% (SC + C_2H), 6%(S + l-C_3H) (*A*-type model). The rest of the trajectories originate (SC_3 + H) through M2.

must point out that, in our previous study of the S + l-C_3H reaction,[18] we bracketed the production of SC_3 + H between 24% and 52% at 300 K, with these limits corresponding to an *A*-type (nonrandom) model and a *C*-type (MNMS) model, respectively. The percentages corresponding to the SC + C_2H channel were 71% (*A*-type model) and 35% (MNMS; see footnote of Table 5). Note that, in the case of the S + l-C_3H reaction, the trajectories were initiated at M1, which implies that the energy distribution models are applied to this species.

It is worthwhile to investigate in more detail the fates of those trajectories evolving through M1 and compare the present results with those obtained for the S + l-C_3H reaction.[18] In general, the percentages of the fragmentation processes of M1 determined with the three models (see the last two rows of Table 5) are much closer to those obtained with the nonrandom model of the S + l-C_3H reaction than with the *C*-type one (see footnote of Table 5). In the present case, we have found that, for model A (B) at 300 K, 13% (10%) of the trajectories dissociate to SC_3 + H and 82% (85%) dissociate to SC + C_2H. For model C the results are 20% of SC_3 + H dissociations and 75% of SC + C_2H dissociations. The differences between the three models may be explained by two facts. First, the normal modes of M2 but the three lowest ones (the two S−C_3H bendings and the S−C_3H stretch) have altogether 72.9 kcal mol^{-1} in model C vs 12.5 (18.5) kcal mol^{-1} in model A (B). Therefore, the C−H terminal stretch has, on average, much more energy in model C than in models A and B. This vibrational mode may not exchange energy very efficiently; as a consequence, the number of C_3−H dissociations of M1 is larger for model C than for the others. It must be noted that M2 has an average lifetime of about 200 fs. Hutchinson et al.[42] studied the vibrational energy flow from an initially excited C−H bond in model hydrocarbon chains. They found that at very high C−H vibrational energies (v > 10) nonlinear resonances[43] lead to irreversible energy flow on a time scale of ca. 100 fs, independent of chain length. At lower energies (v = 2), they observed no energy transfer at all, which agrees with our results because the C−H stretch in M2 is not highly excited (the average v quantum number is lower than 2). However, this comparison must be taken with caution, because in our case other normal modes of M2 are more excited than the C−H stretch.

Second, by a nonstatistical behavior of M1, that is, the intramolecular energy redistribution in M1 is not rapid enough to ensure ergodic behavior. As a result, somewhat different branching ratios are obtained for the three models employed.

The nonstatistical behavior of M1 was also found in our previous study of the S + *l*-C_3H reaction,[18] in which only 6% of the M1 dissociations led to SC_3 + H with nonrandom sampling at the same temperature, whereas 46% led to these products with MNMS.

Process 6 is very often compared to process 1; at $T = 300$ K. it has a percentage of 3% with respect to the total number of trajectories, and a percentage of 5% with respect to the reactions occurred from M1. This value (5%) is in accord with that obtained in our previous study[18] using nonrandom initial conditions (i.e., an *A*-type model), where 7% of the M1 dissociations led to S + *l*-C_3H.

It is important to recall that channel 1 (redissociation of M2 to S + *c*-C_3H) is negligible at the two temperatures studied here and with the three models employed in the phase space sampling of M2. This result together with the fragmentation ratios of M1 suggests that the energy deposited initially in the $S-C_2$ stretch flows rapidly and efficiently to other degrees of freedom, with the likely exception of the C−H stretch. From all these results, we conclude that the process M2 → M1 (through TS12) excites preferentially the $S-C_1$ and C_1-C_2 stretches, with the degrees of freedom associated to the C_2C_3H moiety, especially the C−H stretch, behaving to some extent as spectators. There are at least two reasons for this to be so. First, the C_2C_3H frame has not changed its geometry very much on going from M2 to M1. Second, the C_1-C_3 stretch couples more efficiently with the C_1-C_2 stretch than does with the terminal C−H stretch, which is a very high frequency mode and probably behaves as a local mode. If in the process M2 → M1 most of the energy is trapped on the $S-C_1$ and C_1-C_2 stretches and if these modes exchange the energy efficiently as seen in our previous study,[18] process 5 should be favored over process 4, which requires a large amount of energy in the C−H stretch. This is what is observed in the present study: more than 75% of the trajectories reaching M1 lead to SC + C_2H, which is substantially higher than the 35% obtained with microcanonical sampling of M1 in our previous work.[18] In other words, even if the initial energy distribution of M2 is statistical, M1 is formed with a rather nonstatistical distribution, the reason being the particular form of TS12 that requires some energy accumulation on the $S-C_1$ and C_1-C_2 bonds. However the nonstatistical distribution of M1 generated from M2 is by no means as extreme as the one obtained directly with model A for the S + *l*-C_3H reaction. In particular, the ratios 5/4 (process 5 over process 4) calculated in this study for models A and B are 6.3 and 3.7 respectively, whereas those computed previously for models A and C are 14.2 and 0.9. Besides, the fact that the 5/4 ratios calculated in this study are more similar to each other than the ones computed for the S + *l*-C_3H reaction indicates that the vibrational relaxation must progress more easily in M2 than in M1. However, it is not complete (otherwise the ratios would be virtually equal). Note that only a rapid energy exchange between the $S-C_1$ and C_1-C_2 stretches may explain why the percentage corresponding to the M1 → S + *l*-C_3H fragmentation is mostly independent of the model and equivalent to that found in the S + *l*-C_3H reaction with the nonstatistical model (equivalent to model A), where a very high percentage of the energy was placed in the $S-C_1$ stretch. In fact, the behavior of M1 may be reminiscent of that of N_3H, where the terminal N−N stretch impulses the rupture of the central N−N bond.[44]

Conclusions

We have performed a theoretical dynamical study of the S + *c*-C_3H reaction. It is decomposed in a capture or collision step and an unimolecular step, which have received separate treatments. We have compared the results with those of a similar study of the S + *l*-C_3H reaction.

First of all, it must be pointed out that the capture rate must be almost equal to the overall rate, for the branching ratio corresponding to the generation of S + (*c*,*l*)-C_3H is very small. The capture rate is almost twice that of the S + *l*-C_3H reaction for $T = 300$ K but gets very close to the latter at $T = 60$ K. Second, the branching ratio for the generation of SC_3 must be very close to 50%, with this result being quite independent of the capture or energy distribution model. This ratio could be somewhat higher than the one corresponding to the S + *l*-C_3H reaction, which varies much more with the model and was bracketed between 52% and 24% at $T = 300$ K. In both cases, the competing channel is the generation of SC + C_2H. Finally, both the capture rate and the branching ratios appear not to vary much with temperature, especially the latter quantities. According to these considerations, and subjected, of course, to the abundance of the reactants, one might conclude that the S + *c*-C_3H reaction could be a somewhat more efficient way of producing SC_3 than the S + *l*-C_3H reaction, especially at high temperatures.

We would also like to note as a conclusion that the behavior of the nearly-linear form of SC_3H is critical in the dynamics of this system in both the S + *c*-C_3H and the S + *l*-C_3H reactions. Its behavior might be highly non-RRKM because of (i) an impulsive mechanism which transfers energy rapidly and efficiently from the S−C bond to the next C−C bond, which may break originating SC + C_2H, and (ii) a somewhat inefficient energy exchange between the SC_3 moiety and the C−H bond.

Acknowledgment. J.R.F acknowledges the financial support of the Project BFM2001-3303 granted by the Ministerio de Ciencia y Tecnología, Spain, and the Projects PXI30104PN and PXI30108PR provided by the government of the autonomous region of Galicia. E.M.-N. acknowledges Ministerio de Ciencia y Tecnología, Spain for a Ramón y Cajal research contract, and E.M.-N. and S.A.V. also acknowledge the above ministry for financial support under Project BQU2000-0462. We acknowledge the services provided by the Centro de Computación de Galicia (CESGA).

Appendix

The rotational Hamiltonian of the *c*-C_3H group H_{rot} has been given two equivalent expressions in terms of two sets of Euler angles and their corresponding momenta. The reason of using two alternative expressions is that they become singular for different orientations of the molecule with respect to the space-fixed frame, so one changes from one formulation to the other to avoid this singularity. This procedure was proposed by Kroes and Rettschnick for dealing with the dynamics of formation of He−glyoxal complexes, although they used symmetric rotor Hamiltonians.[45] It is an alternative to the action-variable method of Augustin and Miller.[46] The two sets of Euler angles used are the 313 set $\{\phi,\theta,\psi\}$[47] and the 123 set[45] $\{\alpha,\beta,\gamma\}$. Because we employ the asymmetric-rotor Hamiltonian, it could be of some interest to reproduce the formulas we have employed for the $\{\alpha,\beta,\gamma\}$ set.

The Hamiltonian takes the following form

$$H_{\mathrm{rot}}(p_\alpha,p_\beta,p_\gamma,\beta,\gamma) = \left[\frac{\tan^2\beta}{2}\left(\frac{\cos^2\gamma}{I_x}+\frac{\sin^2\gamma}{I_y}\right)+\frac{1}{2I_z}\right]p_\gamma{}^2 + \frac{1}{2\cos^2\beta}\left[\frac{\cos^2\gamma}{I_x}+\frac{\sin^2\gamma}{I_y}\right]p_\alpha{}^2 + \frac{1}{2}\left[\frac{\sin^2\gamma}{I_x}+\frac{\cos^2\gamma}{I_y}\right]p_\beta{}^2 + -\frac{\tan\beta}{\cos\beta}\left[\frac{\cos^2\gamma}{I_x}+\frac{\sin^2\gamma}{I_y}\right]p_\alpha p_\gamma + \frac{1}{2}\sin(2\gamma)\tan\beta\left[\frac{1}{I_x}-\frac{1}{I_y}\right]p_\beta p_\gamma + \frac{1}{2}\frac{\sin(2\gamma)}{\cos\beta}\left[\frac{1}{I_x}-\frac{1}{I_y}\right]p_\alpha p_\beta \quad (32)$$

and the momenta may be written as follows

$$p_\alpha = I_x(\cos\beta\cos\gamma\dot{\alpha}+\sin\gamma\dot{\beta})\cos\beta\cos\gamma - I_y(\cos\gamma\dot{\beta}-\cos\beta\sin\gamma\dot{\alpha})\cos\beta\sin\gamma + I_z(\sin\beta\dot{\alpha}+\dot{\gamma})\sin\beta$$

$$p_\beta = I_x(\cos\beta\cos\gamma\dot{\alpha}+\sin\gamma\dot{\beta})\sin\gamma + I_y(\cos\gamma\dot{\beta}-\cos\beta\sin\gamma\dot{\alpha})\cos\gamma$$

$$p_\gamma = I_z(\sin\beta\dot{\alpha}+\dot{\gamma}) \quad (33)$$

The transformation between the two sets of Euler angles is given in ref 45. The Hamiltonian reduces to the one given in ref 45 when $I_x = I_y$, but our expression for p_α has a $I_z \sin^2\beta\dot{\alpha}$ term which appears as $I_z\sin\beta\dot{\alpha}$ in that paper; this difference must be the result of a misprint. Also our E_{12} element of the matrix transforming $\{p_\alpha,p_\beta,p_\gamma\}$ into $\{p_\phi,p_\theta,p_\psi\}$ equals to $\sin\theta\sin\psi\sin\gamma + \sin\theta\cos\psi\cos\gamma$ instead of the misprinted expression of ref 45.

References and Notes

(1) Smith, D. *Chem. Rev.* **1992**, *92*, 1473.
(2) Lovas, F. J.; Suenram, R. D.; Ogata, T.; Yamamoto, S. *Astrophys. J.* **1992**, *399*, 325.
(3) Ohshima, Y.; Endo, Y. *J. Mol. Spectrosc.* **1992**, *153*, 627.
(4) Hirahara, Y.; Ohshima, Y.; Endo, Y. *Astrophys. J.* **1993**, *408*, L113.
(5) Kasai, Y.; Obi, K.; Ohshima, Y.; Hiahara, Y.; Endo, Y.; Kawaguchi, K.; Murakami, A. *Astrophys. J.* **1993**, *410*, L45.
(6) Tang, J.; Saito, S.; *J. Mol. Spectrosc.* **1995**, *169*, 92.
(7) Szczepanski, J.; Hodyss, R.; Fuller, J.; Vala, M. *J. Phys. Chem.* **1993**, *97*, 1975.
(8) Maier, G.; Reisenauer, H. P.; Schrot, J.; Janoschek, R. *Angew. Chem. Int. Ed. Engl*. **1990**, *29*, 1464.
(9) Lee, S. *Chem. Phys. Lett.* **1997**, *268*, 69.
(10) Maclagan, R. G. A. R.; Sudkeaw, P. *Chem. Phys. Lett.* **1992**, *194*, 147.
(11) Peeso, D. J.; Ewing, D. W.; Curtis, T. T. *Chem. Phys. Lett*. **1990**, *166*, 307.
(12) Flores, J. R.; Pérez Juste, I.; Carballeira, L.; Estévez, C.; Gómez, F. *Chem. Phys. Lett*. **2001**, *343*, 105.
(13) Murakami, A. *Astrophys. J*. **1990**, *357*, 288.
(14) Seeger, S.; Botschwina, P.; Flügge, J.; Reisenauer, H. P.; Maier, G. *J. Mol. Struct. (THEOCHEM)* **1994**, *303*, 213.
(15) Millar, T. J.; Flores, J. R.; Markwick, A. J. *Mont. Not. R. Astron. Soc*. **2001**, *327*, 1173.
(16) Petrie, S. *Mont. Not. R. Astron. Soc*. **1996**, *281*, 666.
(17) Flores, J. R.; Gómez, F. J. *J. Phys. Chem. A* **2001**, *105*, 10384.
(18) Martínez-Nuñez, E.; Flores, J. R.; Gómez, F. J. In *Femtochemistry and Femtobiology: Ultrafast Dynamics in Molecular Science*; Douhal, A., Santamaria, J., Eds.; World Scientific Publishing: Singapore, 2002, in press.
(19) Stewart, J. P. P. *J. Comput. Chem.* **1989**, *10*, 209.
(20) González-Lafont, A.; Truong, T.; Truhlar, D. G. *J. Phys. Chem.* **1991**, *95*, 4618.
(21) Doubleday, C., Jr.; Bolton, K.; Peslherbe, G. H.; Hase, W. H. *J. Am. Chem. Soc.* **1996**, *118*, 9922.
(22) Doubleday, C., Jr.; Bolton, K.; Peslherbe, G. H.; Hase, W. H. *J. Phys. Chem. A.* **1998**, *102*, 3648.
(23) Bolton, K.; Hase, W. L.; Peslherbe, G. H. In *Modern Methods for Multidimensional Dynamics Computation in Chemistry*; Thompson, D. L., Ed.; World Scientific: Singapore, 1998; p 143.
(24) Fosse, D.; Cernicharo, J.; Gerin, M.; Cox, P. *Astrophys. J.* **2001**, *552*, 168.
(25) Ochsenfeld, C.; Kaiser, R. I.; Lee, Y. T.; Suits, A. G.; Head-Gordon, M. *J. Chem. Phys.* **1997**, *106*, 4141.
(26) Kaiser, R. I.; Oschsenfeld, C.; Head-Gordon, M.; Lee, Y. T.; Suits, A. G. Dep. Chem., University California, Berkeley, CA. *Science* **1996**, *274*, 1508.
(27) Becke, A. D. J. *Chem. Phys*. **1993**, *98*, 5648.
(28) Pople, J. A.; Head-Gordon, M.; Raghavachari, K. *J. Chem. Phys.* **1987**, *87*, 5968.
(29) McLean, A. D.; Chandler, G. S. *J. Chem. Phys.* **1980**, *72*, 5639.
(30) Frisch, M. J.; Trucks, G. W.; Schlegel, H. B.; Scuseria, G. E.; Robb, M. A.; Cheeseman, J. R.; Zakrzewski, V. G.; Montgomery, J. A., Jr.; Stratmann, R. E.; Burant, J. C.; Dapprich, S.; Millam, J. M.; Daniels, A. D.; Kudin, K. N.; Strain, M. C.; Farkas, O.; Tomasi, J.; Barone, V.; Cossi, M.; Cammi, R.; Mennucci, B.; Pomelli, C.; Adamo, C.; Clifford, S.; Ochterski, J.; Petersson, G. A.; Ayala, P. Y.; Cui, Q.; Morokuma, K.; Malick, D. K.; Rabuck, A. D.; Raghavachari, K.; Foresman, J. B.; Cioslowski, J.; Ortiz, J. V.; Stefanov, B. B.; Liu, G.; Liashenko, A.; Piskorz, P.; Komaromi, I.; Gomperts, R.; Martin, R. L.; Fox, D. J.; Keith, T.; Al-Laham, M. A.; Peng, C. Y.; Nanayakkara, A.; Gonzalez, C.; Challacombe, M.; Gill, P. M. W.; Johnson, B. G.; Chen, W.; Wong, M. W.; Andres, J. L.; Head-Gordon, M.; Replogle, E. S.; Pople, J. A. *Gaussian 98*; Gaussian, Inc.: Pittsburgh, PA, 1998.
(31) Curtiss, L. A.; Carpenter, J. E.; Raghavachari, K.; Pople, J. A. *J. Chem. Phys.* **1987**, *87*, 5968.
(32) Dateo, C. E.; Clary, D. C. *J. Chem. Phys*. **1989**, *90*, 7216.
(33) Jacox, M. E. *Vibrational and Electronic Energy Levels of Polyatomic Transient Molecules* in NIST Chemistry WebBook, NIST Standard Reference Database Number 69; Mallard, W. G., Linstrom, P. J., Eds.; National Institute of Standards and Technology: Gaithersburg, MD, February 2000 (http://webbook.nist.gov).
(34) Flores, J. R.; Gómez, F. J. *Mol. Phys*. **2002**, *100*, 569.
(35) Pack, R. T. *J. Chem. Phys*. **1974**, *60*, 633.
(36) Buckingham, A. D. In *Intermolecular Forces*; Hirschfelder, J. O., Ed.; John Wiley & Sons: New York, 1967.
(37) The quadrupole components correspond to the following definition $\Theta_{ij} = (1/2)\sum_m e_m(3r_{i,m}r_{j,m} - \delta_{ij}r_m^2)$.
(38) Flores, J. R.; Estévez, C. M.; Pérez I.; Carballeira, L. *J. Phys. Chem. A* **2001**, *105*, 4716.
(39) Hase, W. L.; Buckowski, D. G. *Chem. Phys. Lett.* **1980**, *74*, 284.
(40) Thompson, D. L. GENDYN program.
(41) Stewart, J. P. P. *MOPAC7.0*, a General Molecular Orbital Package; QCPE, 1993; p 455.
(42) Hutchinson, J. S.; Reinhardt, W. P.; Hynes, J. P. *J. Chem. Phys*. **1983**, *79*, 4247.
(43) Hutchinson, J. S. In *Advances in Classical Trajectory Methods*; Hase, W. L., Ed.; Jai Press Inc.: London, 1992; Vol. 1.
(44) Hutchinson, J. S. In *Dynamics of Molecules and Chemical Reactions*; Wyatt, R. E., Zhang, J. Z. H., Eds.; Marcell Dekker: New York, 1996.
(45) Kroes, G.-J.; Rettschnick, R. P. H. *J. Chem. Phys*. **1989**, *91*, 1556.
(46) Augustin, S. D.; Miller, W. H. *J. Chem. Phys*. **1974**, *61*, 3155.
(47) Goldstein, H. *Classical Mechanics*; Addison-Wesley: New York, 1980.